Evaluation of plastic materials for range shifting, range compensation, and solid-phantom dosimetry in carbon-ion radiotherapy[a)]

Nobuyuki Kanematsu,[b)] Yusuke Koba, and Risa Ogata
Research Center for Charged Particle Therapy, National Institute of Radiological Sciences, 4-9-1 Anagawa, Inage-ku, Chiba 263-8555, Japan

(Dated: November 2012—April 2013, Reprint: 30 September 2016)

Purpose: Beam range control is the essence of radiotherapy with heavy charged particles. In conventional broad-beam delivery, fine range adjustment is achieved by insertion of range shifting and compensating materials. In dosimetry, solid phantoms are often used for convenience. These materials should ideally be equivalent to water. In this study, we evaluated dosimetric water equivalence of four common plastics, HDPE, PMMA, PET, and POM.

Methods: Using the Bethe formula for energy loss, the Gottschalk formula for multiple scattering, and the Sihver formula for nuclear interactions, we calculated the effective densities of the plastics for these interactions. We experimentally measured variation of the Bragg peak of carbon-ion beams by insertion of HDPE, PMMA, and POM, which were compared with analytical model calculations.

Results: The theoretical calculation resulted in slightly reduced multiple scattering and severely increased nuclear interactions for HDPE, compared to water and the other plastics. The increase in attenuation of carbon ions for 20-cm range shift was experimentally measured to be 8.9% for HDPE, 2.5% for PMMA, and 0.0% for POM while PET was theoretically estimated to be in between PMMA and POM. The agreement between the measurements and the calculations was about 1% or better.

Conclusions: For carbon-ion beams, POM was dosimetrically indistinguishable from water and the best of the plastics examined in this study. The poorest was HDPE, which would reduce the Bragg peak by 0.45% per 1-cm range shift, although with marginal superiority for reduced multiple scattering. Between the two clear plastics, PET would be superior to PMMA in dosimetric water equivalence.

PACS numbers: 87.67.ng, 87.57.uq, 82.35.Lr, 27.20+n
Keywords: range shifter, range compensator, nuclear interactions, tissue equivalency, heavy ions

I. INTRODUCTION

The essence of radiotherapy with heavy charged particles is its intrinsic capability of three-dimensional dose formation with a Bragg peak at the beam range, which can be precisely controlled by adapting the beam energy incident on a patient. In conventional broad-beam delivery,[1,2] a range shifter degrades excessive beam energy and a range compensator fills target-depth deficit varying in the field to best conform the spread-out Bragg peak to a planning target volume.[3]

A range shifter is typically a composite of plates of precisely controlled thickness and a range compensator is a physical filter custom-made for an individual field. Their material should be uniform, stable, machinable, inexpensive, and ideally equivalent to water, which is the reference material for dosimetry. These requirements are also valid for solid phantom materials, which are used when water-phantom dosimetry is not possible or convenient. To estimate the effective thickness of a material by the resultant range shift in water, an effective density is assigned for the material. However, this approximation may cause dosimetric errors due to alteration of the radiation because the effective density differs for multiple scattering and nuclear interactions.[4] Dosimetric water equivalence, which is evaluated by uniformity of effective densities for relevant interactions, is essential to energy degrading of charged-particle beams for range shifting, range compensation, and dosimetry.

Some common materials used for this purpose are high-density polyethylene (HDPE),[5] polymethyl methacrylate (PMMA),[3] and synthetic resin of acrylonitrile, butadiene, and styrene (ABS).[6] In general, HDPE is inexpensive and close to water in density, PMMA is good at dimensional stability and contains oxygen which is dominant in water, and ABS is available in various forms in industry as chemical wood. For proton and ion-beam dosimetry, PMMA has been commonly used as a water-equivalent phantom material.[7,8]

In the past, water equivalence of general plastics (PMMA, HDPE, PS, and PTFE), tissue-substitute plastics (A150 and commercial products), and other solid materials (graphite, bone, aluminum, and copper) have been studied for energy degrading and calorimetry of proton and ion beams by experiment and Monte Carlo simulation.[9–13] Those studies primarily focused on

[a)] This study has been published in Medical Physics 40(4) 041724, April 2013 (http://dx.doi.org/10.1118/1.4795338).
[b)] nkanemat@nirs.go.jp

TABLE I. Material properties (elemental composition, oxygen weight fraction w_8, typical density ρ, number of electrons per atomic mass unit $\langle Z/A_r\rangle$, and mean excitation energy I) excerpted from Ref. 15 (also available at the Particle Data Group website) except for an empirical HDPE density.

Material	Composition	w_8	$\rho/(\mathrm{g/cm^3})$	$\langle Z/A_r\rangle$	I/eV
HDPE	$(C_2H_4)_n$	0.000	0.96	0.57034	57.4
PMMA	$(C_5H_8O_2)_n$	0.320	1.19	0.53937	74.0
PET	$(C_{10}H_8O_4)_n$	0.333	1.40	0.52037	78.7
POM	$(CH_2O)_n$	0.533	1.42	0.53287	77.4
Water	H_2O	0.888	1.00	0.55509	79.7

fluence-correction factor, which is the ratio of dose in water to dose-to-water in material of interest at a same water-equivalent depth. While the fluence-correction factor is essential for dosimetry with non-water phantom, generalization for a variety of modulated treatment beams may be difficult due to varied dose contribution from secondary particles and atomic recoils.

For carbon-ion radiotherapy, the radiation components need to be handled separately due to variability of relative biological effectiveness with particle charge and energy,[14] for which the fluence-correction factor for total dose would not suffice. Instead, survival of carbon ions that attenuate with depth to form a Bragg peak could be clinically more relevant. In this regard, we evaluate water equivalence of some plastics for energy degrading of carbon-ion beams.

II. MATERIALS AND METHODS

A. Sample plastics

In addition to HDPE and PMMA, we theoretically evaluated two other oxygen-rich plastics, polyethylene terephthalate (PET) and polyoxymethylene (POM), among which we experimentally tested HDPE, PMMA, and POM with carbon-ion beams. We excluded ABS as it varies in composition of carbon, hydrogen, and nitrogen. Table I summarizes the relevant properties of these plastics and water,[15] in which the densities may vary with degree of polymerization. Incidentally, $n_e = \langle Z/A_r\rangle\,\rho/u$ is the electron density, where u is the atomic mass unit.

B. Effective densities for ion-beam Interactions

1. Stopping-power ratio

Stopping power S of a material for energetic charged particles is given by the Bethe theory.[16] The effective density for energy degrading is the stopping-power ratio of material to water, which is defined as

$$\frac{S}{S_w} = \frac{\langle Z/A_r\rangle\,\rho}{\langle Z/A_r\rangle_w\,\rho_w}\,\frac{\ln\frac{2m_ec^2}{I} + \ln\frac{v^2}{c^2-v^2} - \frac{v^2}{c^2}}{\ln\frac{2m_ec^2}{I_w} + \ln\frac{v^2}{c^2-v^2} - \frac{v^2}{c^2}}, \tag{1}$$

where ρ, $\langle Z/A_r\rangle$, and I for plastics and ρ_w, $\langle Z/A_r\rangle_w$, and I_w for water are given in Table I, m_e is the electron mass, and v and c are the particle speed and the light speed in vacuum. The v-dependence of S/S_w is small for plastics with $I \approx I_w$. For example, S/S_w varies by $+0.9\%$ for slowing down in HDPE ($I/I_w = 72\%$) from $v^2/c^2 = 0.5$ ($E/A = 385.8$ MeV) to $v^2/c^2 = 0.1$ ($E/A = 50.4$ MeV), where E/A is the kinetic energy per nucleon. By representing the particle speed with $v^2/c^2 = 0.5$ in this study, the stopping-power ratio was approximated to be energy independent as

$$\frac{S}{S_w} \approx \frac{\langle Z/A_r\rangle\,\rho}{\langle Z/A_r\rangle_w\,\rho_w}\,\frac{\ln\frac{2m_ec^2}{I} - 0.5}{\ln\frac{2m_ec^2}{I_w} - 0.5}, \tag{2}$$

on which the influence of I-value uncertainty is generally small. For example, 3% change of I_w will cause only 0.3% effect to S/S_w. Incidentally, International Commission on Radiation Units and Measurements (ICRU) tentatively recommended $I_w = 78$ eV for water,[17] which deviates by -1.7 eV from the value in Table I.

Alternatively, without depending on these uncertain ρ and I values, the stopping-power ratio can be directly measured by range shift s in water per material thickness t inserted upstream of water,

$$\frac{S}{S_w} \approx \frac{s}{t}, \tag{3}$$

ignoring the air ($\rho/\rho_w \approx 0.1\%$) that is replaced by the inserted material.

2. Scattering-power ratio

The effective density for multiple scattering is the scattering-power ratio of material to water. Using the scattering-power formula for heavy charged particles by Gottschalk,[18] it is defined as

$$\frac{T}{T_w} = \frac{\rho}{91.69\rho_w}\sum_i \frac{w_i}{A_{\mathrm{r}i}}Z_i^2\left(29.73 - \ln Z_i - \ln A_{\mathrm{r}i}\right), \tag{4}$$

where Z_i, A_{ri}, and w_i are the atomic number, the atomic weight, and the weight fraction of element i.

For range shift s, the increase of mean square angle of the primary particles in the material differs from that in water by a double-ratio factor,

$$\Delta\overline{\theta^2}(s) = \frac{T/T_w}{S/S_w}\Delta\overline{\theta^2}_w(s). \tag{5}$$

The increase of mean square angle in water can be estimated by a semi-empirical formula,[19]

$$\Delta\overline{\theta^2}_w(s) = \frac{1.00}{1000}\,z^{-0.16}\left(\frac{m}{m_p}\right)^{-0.92}\ln\frac{R_0}{R_0 - s}, \tag{6}$$

for particles of range R_0, charge ze, and mass m, where e is the elementary charge and m_p is the proton mass.

3. Nuclear-cross-section ratio

In the Sihver model,[20] the geometrical cross section for collision between a projectile nucleus of mass number A and a target nucleus of element i is given by

$$\sigma_{Ai} = \pi r_0^2 \left[A^{\frac{1}{3}} + {A_r}_i^{\frac{1}{3}} - b_{0Ai} \left(A^{-\frac{1}{3}} + {A_r}_i^{-\frac{1}{3}} \right) \right]^2, \quad (7)$$

where $r_0 = 1.36$ fm is the effective nucleon radius and b_0 is the transparency parameter, for which the proton–nucleus formula is applied for collisions on hydrogen ($i = 1$), namely

$$b_{0Ai} = \begin{cases} 2.247 - 0.915 \left(A^{-\frac{1}{3}} + {A_r}_i^{-\frac{1}{3}} \right) & \text{for } i = 1 \\ 1.581 - 0.876 \left(A^{-\frac{1}{3}} + {A_r}_i^{-\frac{1}{3}} \right) & \text{for } i > 1. \end{cases} \quad (8)$$

The effective density for nuclear interactions is the nuclear-cross-section ratio of material to water,

$$\frac{\sigma_A}{\sigma_{Aw}} = \frac{\langle \sigma_A / A_r \rangle \, \rho}{\langle \sigma_A / A_r \rangle_w \, \rho_w}, \quad (9)$$

where

$$\langle \sigma_A / A_r \rangle = \sum_i \frac{w_i}{A_{ri}} \sigma_{Ai} \quad (10)$$

is the nuclear cross section per atomic mass unit of the material. The energy dependence of the nuclear-cross-section ratio may be reasonably ignored due to cancellation of common energy dependence for $E/A \gtrsim 100$ MeV expected in the Sihver model.

Number of primary particles N decreases in matter due to nuclear interactions. With an insert for range shift s, the number at depth d in water is factorized as

$$N(d) = \alpha(s) \, N_w(s + d), \quad (11)$$

where $N_w(d)$ is the number of primary particles at depth d in water for $s = 0$ and survival ratio $\alpha(s) = N(0)/N_w(s)$ is the ratio of the number of carbon ions after range shift s to that in water at depth $d = s$. The fractional attenuation per range shift, $(-dN/ds)/N$, differs between the material and water by a double-ratio factor,

$$-\frac{1}{N}\frac{dN}{ds} = \frac{\sigma_A/\sigma_{Aw}}{S/S_w} \left(-\frac{1}{N}\frac{dN}{ds} \right)_w, \quad (12)$$

which is solved with boundary condition $N = N_w$ for $s = 0$, resulting in

$$\alpha(s) = \left(\frac{N_w(d = s)}{N_w(d = 0)} \right)^{\frac{\sigma_A/\sigma_{Aw}}{S/S_w} - 1}. \quad (13)$$

If we employ an empirical formula for attenuation of carbon ions in water described in Appendix with substitution of residual range $R = R_0 - s$, the survival ratio in the exponential region ($s \le R_0 - 2$ cm) reduces to

$$\alpha(s) = \exp\left(-\frac{s}{25.5 \text{ cm}} \left(\frac{\sigma_{12}/\sigma_{12w}}{S/S_w} - 1 \right) \right), \quad (14)$$

which analytically gives the carbon-ion survival in the plastic relative to that in water.

C. Experiment with carbon-ion beams

The dosimetric water equivalence of different materials should be evaluated by equality of the resultant doses. As far as the primary particles are concerned, the Bethe theory for energy loss and the Molière theory for multiple scattering are accurate to the level of measurement limit if only the ρ and I values are adjusted to a specific material.[16,18] On the contrary, the nuclear-interaction models generally use assumptions, approximations, and extensive cross-section data with finite uncertainties and limitations. Although the model used in this study has been tested,[21] specific validation may be necessary for this particular application.

We conducted an experiment with carbon-ion beams of $E/A = 290$ and 430 MeV extracted from Heavy Ion Medical Accelerator in Chiba (HIMAC) of National Institute of Radiological Sciences. The beams were laterally broadened by a wobbling/scattering system to form a uniform field of 10-cm diameter,[22] longitudinally moderated by a ripple filter for Gaussian range modulation of 1.8 mm (rms),[23] and delivered horizontally to a box-shaped water tank on a movable treatment couch.

We used binary plates of HDPE, PMMA, and POM, which were stacked at the immediate upstream of the tank to construct an insert of arbitrary thickness t in steps of 1 cm. To eliminate the influence of beam divergence for wobbling at about 10 m upstream, the treatment couch was moved downstream so that the Bragg peak would stay in the same place in the laboratory system. The amount of couch movement was the expected range shift $s = (S/S_w)\, t$ using our standard S/S_w values 1.02 for HDPE, 1.16 for PMMA, and 1.36 for POM. The central-axis doses at varied depth d in water after the tank wall of 19-mm PMMA were measured with a Markus-type (PTW Type 23343) plane-parallel ionization chamber (PPIC) with a protective cover of 0.87-mm PMMA, as shown in Fig. 1. The dosimetric precisions were as good as 0.1% for peak dose and 0.1 mm for depth in reproducibility.

We chose insert thicknesses that approximately corresponded to range shifts of 4 cm and 8 cm for 290 MeV and 10 cm and 20 cm for 430 MeV. For beam deliveries of equal monitor units, the central-axis doses were measured at minimum depth intervals of 0.1 mm. For the reference depth of the moderated Bragg peak, we adopted depth d_{80}, at which the dose decreased to 80%

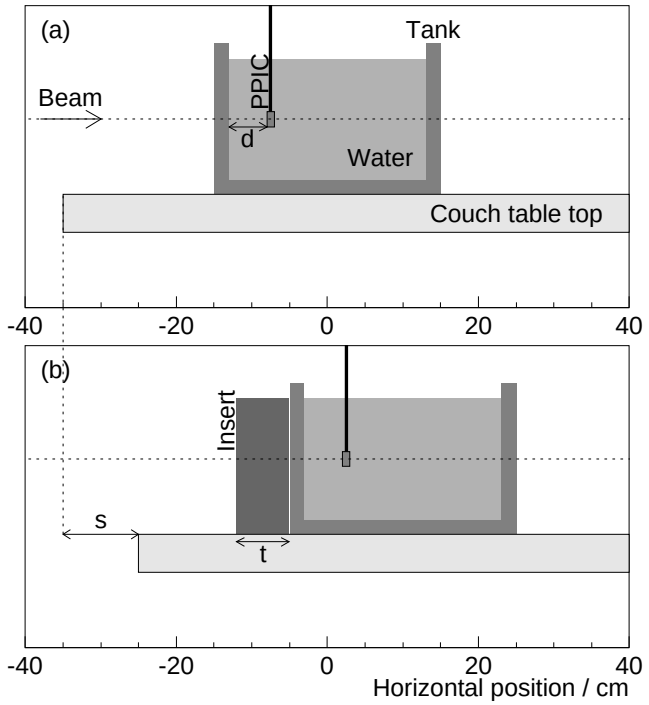

FIG. 1. Side views of apparatus for carbon-ion-beam experiment, (a) for the reference condition and (b) with a plastic insert of thickness t and couch movement by range shift s, where the central-axis (horizontal-dotted-line) doses at varied depth d were measured with PPIC.

of peak dose D_p. Range shift s was measured as the shift of d_{80} by insertion. Using the dose points in the depth region of $d_{80} + 1$ cm $\lesssim d \lesssim d_{80} + 2$ cm, we estimated the fragment dose D_f by extrapolation of the linear-fit line to $d = d_{80}$, for which we assumed the linearity over a few centimeters and ignored small dose variation over about 2 mm between the peak and 80% depths. Taking the beam without insert ($s = 0$) as a reference, the carbon-ion-survival ratios were estimated by reduction of the carbon-ion dose contribution,

$$\alpha(s) = \frac{D_p(s) - D_f(s)}{D_p(0) - D_f(0)}, \tag{15}$$

which were then compared with the analytical model calculations.

III. RESULTS

A. Theoretical effective densities

Table II shows the resultant effective-density calculations in a format insensitive to ρ variation. The dosimetric water equivalence, that is the uniformity of effective densities for the relevant interactions, was highly correlated with the oxygen content of these plastics.

TABLE II. Theoretical double ratios of plastics to water (with subscript w) between density ρ, electron density n_e, stopping power S, scattering power T, and carbon-ion nuclear cross section σ_{12}.

Material	$\frac{n_e}{n_{e\,w}}/\frac{\rho}{\rho_w}$	$\frac{S}{S_w}/\frac{\rho}{\rho_w}$	$\frac{T}{T_w}/\frac{S}{S_w}$	$\frac{\sigma_{12}}{\sigma_{12\,w}}/\frac{S}{S_w}$
HDPE	1.027	1.065	0.712	1.114
PMMA	0.972	0.980	0.890	1.044
PET	0.937	0.939	0.953	1.011
POM	0.960	0.963	0.968	1.004

For HDPE of $\rho = 0.96$ g/cm^3, although its electron-density ratio $n_e/n_{ew} = 0.985$ and stopping-power ratio $S/S_w = 1.020$ are close to 1, it differs from water by -29.0% in multiple scattering and $+11.0\%$ in nuclear interactions. Equation (14) leads to the fractional attenuation ratios per range shift of $(-d\alpha/ds)/\alpha = 0.45\%$/cm for HDPE, 0.17%/cm for PMMA, 0.04%/cm for PET, and 0.02%/cm for POM, which indicate the differences from water in attenuation.

B. Experimental dose variation

Figure 2 shows explicit cases for variation of the moderated Bragg peak by material insertion, with which the peak and fragment doses were measured. The resultant measurements are shown in Table III, where available range R_0 is a sum of the effective thickness of the tank wall, that of the PPIC cover, and the range-equivalent depth measured for $s = 0$. For proton beams with large range straggling, 80%-dose depth d_{80} is commonly used as the range-equivalent depth.[24] For the moderated Bragg peak formed by the stopping carbon ions, fragment contribution D_f/D_p was excluded to redefine the range-equivalent depth with modified relative dose $(1 - D_f/D_p) \times 80\% + D_f/D_p$, which was 82% for 290 MeV and 84% for 430 MeV.

Figure 3 shows the measured and calculated survival ratios for range shift by these plastics. Invariance of the Bragg peak is essential for treatment planning and delivery systems based on water-phantom dosimetry. The reduction of the fragment-subtracted Bragg peak was 8.9% with HDPE for 20-cm range shift to a carbon-ion beam of 28.23-cm range while it was 2.5% with PMMA and 0.0% with POM. The dominant source of uncertainty may be the fragment dose estimated by linear extrapolation of tail doses sampled at a few depths, which would have caused $\lesssim 1\%$ effect to the subtracted peak dose. In fact, the analytical model calculations reasonably agreed with the measurements within 1% in survival ratio.

IV. DISCUSSION

As the density of polymer plastics depends on manufacturing condition, the effective density must be ex-

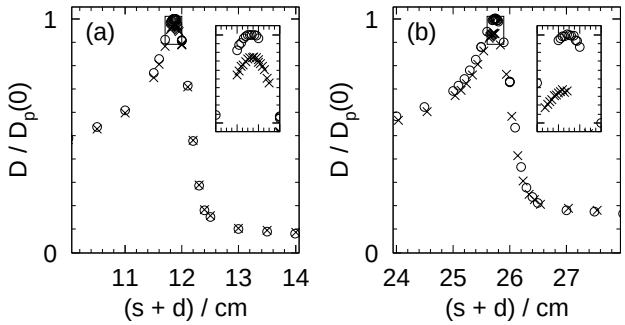

FIG. 2. Depth–dose distributions of the moderated carbon-ion Bragg peak with (×) and without (◯) insertion of (a) 8-cm HDPE for 290 MeV and (b) 20-cm HDPE for 430 MeV, with embedded magnified plots.

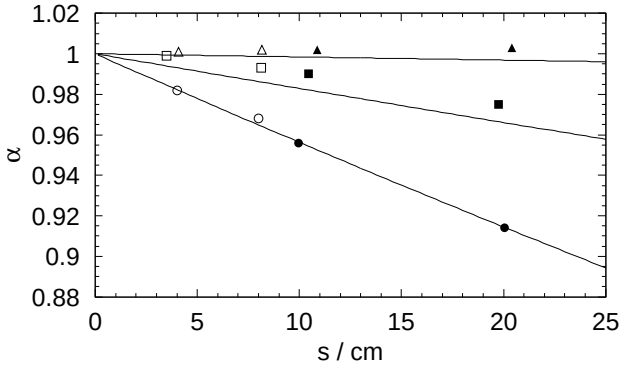

FIG. 3. Carbon-ion survival ratio α measured as Bragg-peak reduction for range shift s by HDPE (circles), PMMA (squares), and POM (triangles) for 290-MeV (open symbols) and 430-MeV (filled symbols) beams along with analytical model curves (solid lines).

TABLE III. Experimental results for carbon-ion attenuation by plastic inserts, showing acceleration energy E/A, available range R_0, material thickness t, range shift s, 80%-dose depth d_{80}, relative peak and fragment doses D_p and D_f, and carbon-ion-survival ratio α.

$E/A = 290$ MeV			$R_0 = 14.36$ cm			
Material	t/cm	s/cm	d_{80}/cm	D_p	D_f	α
(Reference)	0	0	12.06	1	0.115	1
HDPE	4	4.02	8.04	0.987	0.118	0.982
	8	8.00	4.06	0.974	0.117	0.968
PMMA	3	3.48	8.58	0.998	0.114	0.999
	7	8.14	3.92	0.992	0.113	0.993
POM	3	4.09	7.97	1.000	0.114	1.001
	6	8.17	3.89	1.001	0.114	1.002
$E/A = 430$ MeV			$R_0 = 28.23$ cm			
Material	t/cm	s/cm	d_{80}/cm	D_p	D_f	α
(Reference)	0	0	25.95	1	0.199	1
HDPE	10	9.97	15.98	0.966	0.200	0.956
	20	20.04	5.91	0.937	0.205	0.914
PMMA	9	10.45	15.50	0.992	0.199	0.990
	17	19.75	6.20	0.981	0.200	0.975
POM	8	10.88	15.07	1.001	0.198	1.002
	15	20.42	5.53	0.999	0.195	1.003

perimentally determined before its clinical use to an accuracy better than 1%. Therefore, the stopping-power similarity to water ($S \approx S_w$) for HDPE is not essentially an advantage. The similarity is only relevant when geometrical dose properties are of interest, such as field width and penumbra size. For applications that allow or require regular air gaps in a phantom, higher S/S_w values are acceptable or may even be preferable. For example, Yajima *et al.* developed a multilayer ionization chamber composed of 3-mm and 4-mm PMMA plates interleaved with 1-mm air gaps,[8] which would reduce the density by factor 7/9 resulting in mean stopping-power ratio $\langle S/S_w \rangle = 0.90$. If POM is used instead, the $\langle S/S_w \rangle$ value will be 1.06, which will further be adjusted to 1.00 by extending the air gaps to 1.26 mm.

Beam blurring due to multiple scattering in a range compensator should ideally be minimized. In this regard, HDPE with $(T/T_w)/(S/S_w) = 0.712$ is superior to PMMA (0.890), PET (0.953), POM (0.968), and water (1) although their effective differences will be generally marginal. For example, when a carbon-ion beam of 20-cm available range traverses a plastic plate for 10-cm range shift, the induced beam blurring in 30-cm distance will be 1.9 mm for HDPE, 2.1 mm for PMMA, 2.2 mm for PET, and 2.2 mm for POM, using Eqs. (5) and (6).

The dosimetric water equivalence of the plastics that we tested here originated from the similarity with water in oxygen content and should be also valid for protons and other ions. Therefore, POM will be generally a good dosimetric material if its high density is tolerable. For some dosimetric applications that require material transparency, such as water tank with optical dosimeter-alignment system, PET may desirably substitute for PMMA.

V. CONCLUSIONS

We evaluated dosimetric water equivalence of four common plastics, HDPE, PMMA, PET, and POM, by uniformity of effective densities for carbon-ion-beam interactions. Among them, POM was the best and virtually indistinguishable from high-density water, which would be ideal for range control and preferable for dosimetry with regular air gaps such as for multilayer ionization chamber. For applications that require transparency such as water tank with optical dosimeter-alignment system, PMMA was verified to be reasonably water equivalent and PET would be even better. The poorest was HDPE with a large fractional attenuation ratio of 0.45% per 1-cm range shift, although with marginal

superiority for reduced multiple scattering. Analytical model calculations agreed with measurements within 1% for carbon-ion-survival ratio of plastic to water. The water equivalence of plastics was highly correlated with their oxygen content, as expected from the composition of water.

Appendix: Attenuation of carbon ions in water

Haettner *et al.* measured the number of carbon ions, N_w, attenuating with depth d in water for $E/A = 200$ MeV and 400 MeV.[25] We compiled their data to construct an energy-independent universal formula as a function of residual range in water, $R = d_R - d$, where d_R is the range-equivalent depth.

Using the measured $N_w(d)$ curve for each energy, the d_R was tentatively set to the maximum-gradient depth. Using the data points for $d_R + 0.5$ cm $< d < d_R + 2$ cm, a straight line was fitted and its intercept at $d = d_R$ was defined as the number of stopped carbon ions, N_{wR}. The d_R was then redefined with submillimeter adjustment to meet $N_w(d_R) = N_{wR}/2$.

The measurements showed natural exponential behavior for $R > 5$ cm, for which we determined the mean free path using the 400-MeV dataset. While there would naturally be some difference between the energies in the small region of $R < 1$ cm due to marginal variation of range straggling, systematic deviation was observed unexpectedly in the larger region of $R < 5$ cm. As the exponential behavior held in the intermediate region of 2 cm $< R < 5$ cm for the 200-MeV dataset, the deviation may be attributed to increased measurement difficulty for the 400-MeV beam. Therefore, we rescaled the 400-MeV dataset to match the 200-MeV dataset in the exponential region of $R > 5$ cm and we adopted the straight line fitted to the 200-MeV dataset for the $R \leq 2$ cm region. The resultant universal formula for carbon-ion attenuation is

$$\frac{N_w(R)}{N_{wR}} = \begin{cases} 1 + \dfrac{R}{11.1 \text{ cm}} & \text{for } R \leq 2 \text{ cm} \\ 1.091 \exp\left(\dfrac{R}{25.5 \text{ cm}}\right) & \text{for } R > 2 \text{ cm}, \end{cases} \quad \text{(A.1)}$$

which is shown in Fig. 4 along with the measurements rescaled as described above.

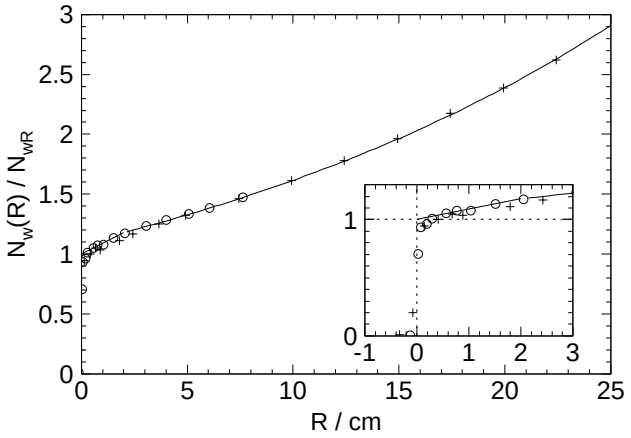

FIG. 4. Number of carbon ions, N_w, per number of stopped carbon ions, N_{wR}, as a function of residual range in water, R, measured by Haettner *et al.*[25] for $E/A = 200$ MeV (◯) and 400 MeV (+) with the fitted function (solid line).

[1] A. M. Koehler, R. J. Schneider, and J. M. Sisterson, "Flattening of proton dose distribution for large-field radiotherapy," Med. Phys. **4** 297–301 (1977).

[2] T. Kanai, M. Endo, S. Minohara, N. Miyahara, H. Koyama-Ito, H. Tomura, N. Matsufuji, Y. Futami, A. Fukumura, T. Hiraoka, Y. Furusawa, K. Ando, M. Suzuki, F. Soga, and K. Kawachi, "Biophysical characteristics of HIMAC clinical irradiation system for heavy-ion radiation therapy," Int. J. Radiat. Oncol. Biol. Phys. **44**, 201–210 (1999).

[3] M. S. Wagner, "Automated range compensation for proton therapy," Med. Phys. **9** 749–752 (1982).

[4] N. Kanematsu, T. Inaniwa, and Y. Koba, "Relationship between electron density and effective densities of body tissues for stopping, scattering, and nuclear interactions of proton and ion beams," Med. Phys. **39** 1016–1020 (2012).

[5] N. Kanematsu, M. Torikoshi, M. Mizota, and T. Kanai, "Secondary range shifting with range compensator for reduction of beam data library in heavy-ion radiotherapy," Med. Phys. **34** 1907–1910 (2007).

[6] Y. Takada, T. Himukai, K. Takizawa, Y. Terashita, S. Kamimura, H. Matsuda, K. Hotta, R. Kohno, M. Komori, and T. Kanai, "The basic study of a bi-material range compensator for improving dose uniformity for proton therapy," Phys. Med. Biol. **53** 5555–5569 (2008).

[7] C. Brusasco, B. Voss, D. Schardt, M. Krämer, and G. Kraft, "A dosimetry system for fast measurement of 3D depth-dose profiles in charged-particle tumor therapy with scanning techniques," Nucl. Instrum. Methods B **168** 578–592 (2000).

[8] K. Yajima, T. Kanai, Y. Kusano, and T. Shimojyu, "Development of a multi-layer ionization chamber for heavy-ion radiotherapy," Phys. Med. Biol. **54** N107–N114 (2009).

[9] H. Palmans, J. E. Symons, J-M. Denis, E. A. de Kock, D. T. L. Jones, and S. Vynckier,"Fluence correction factors in plastic phantoms for clinical proton beams," Phys. Med. Biol. **47** 3055–3071 (2002).

[10] U. Schneider, P. Pemler, J. Besserer, M. Dellert, M. Moosburger, J. de Boer, E. Pedroni, and T. Boehringer, "The water equivalence of solid materials used for dosimetry with small proton beams," Med. Phys. **29** 2946–2951 (2002).

[11] L. Al-Sulaiti, D. Shipley, R. Thomas, A. Kacperek, P. Regan, and H. Palmans, "Water equivalence of various materials for clinical proton dosimetry by experiment and Monte Carlo simulation," Nucl. Instrum. Meth. A **619** 344–347 (2010).

[12] A. Lühr, D. C. Hansen, N. Sobolevsky, H. Palmans, S. Rossomme, and N. Bassler, "Fluence correction factors and stopping power ratios for clinical ion beams," Acta Oncol. **50** 797–805 (2011).

[13] L. Al-Sulaiti, D. Shipley, R. Thomas, P. Owen, A. Kacperek, P. Regan, and H. Palmans, "Water equivalence of some plastic-water phantom materials for clinical proton beam dosimetry," Appl. Radiat. Isotop. **70** 1052–1055 (2012).

[14] Y. Kase, N. Kanematsu, T. Kanai, and N. Matsufuji, "Biological dose calculation with Monte Carlo physics simulation for heavy-ion radiotherapy," Phys. Med. Biol. **51** N467–N475 (2006).

[15] D. E. Groom, N. V. Mokhov, and S. I. Striganov,"Muon stopping-power and range tables, 10 MeV-100 TeV," Atomic Data and Nuclear Data Tables **78** 183–356 (2001).

[16] S. M. Cohen, "Bethe stopping power theory for heavy-element targets and relativistic projectiles," Phys. Rev. A **68** 012720-1–

012720-14 (2003).
[17] P. Sigmund, A. Schinner, and H. Paul, "Errata and addenda for ICRU Report 73, stopping of ions heavier than helium, Journal of the ICRU vol. 5 no. 1 (2005)," available at the ICRU website (2009).
[18] B. Gottschalk, "On the scattering power of radiotherapy protons," Med. Phys. **37** 352–367 (2010).
[19] N. Kanematsu, "Semi-empirical formulation of multiple scattering for the Gaussian beam model of heavy charged particles stopping in tissue-like matter," Phys. Med. Biol. **54** N67–N73 (2009).
[20] L. Sihver, C. H. Tsao, R. Silberberg, T. Kanai, and A. F. Barghouty, "Total reaction and partial cross section calculations in proton–nucleus ($Z_t \leq 26$) and nucleus–nucleus reactions (Z_p and $Z_t \leq 26$)," Phys. Rev. C **47** 1225–1236 (1993).
[21] L. Sihver and D. Mancusi, "Present status and validation of HIBRAC," Radiation Measurements **44** 38–46 (2009).
[22] M. Torikoshi, S. Minohara, N. Kanematsu, M. Komori, M. Kanazawa, K. Noda, N. Miyahara, H. Ito, M. Endo, and T. Kanai, "Irradiation System for HIMAC," J. Radiat. Res. (Tokyo) **48** (Suppl. A) A15–A25 (2007).
[23] B. Schaffner, T. Kanai, Y. Futami, M. Shimbo, and E. Urakabe, "Ridge filter design and optimization for the broad-beam three-dimensional irradiation system for heavy-ion radiotherapy," Med. Phys. **27** 716–724 (2000).
[24] T. Bortfeld, "An analytical approximation of the Bragg curve for therapeutic proton beams," Med. Phys. **24** 2024–33 (1997).
[25] E. Haettner, H. Iwase, and D. Schardt, "Experimental fragmentation studies with ^{12}C therapy beams," Radiat. Prot. Dosim. **122** 485–487 (2006).